JOURNAL OF POLYMER SCIENCE | PART B

Polymer Physics

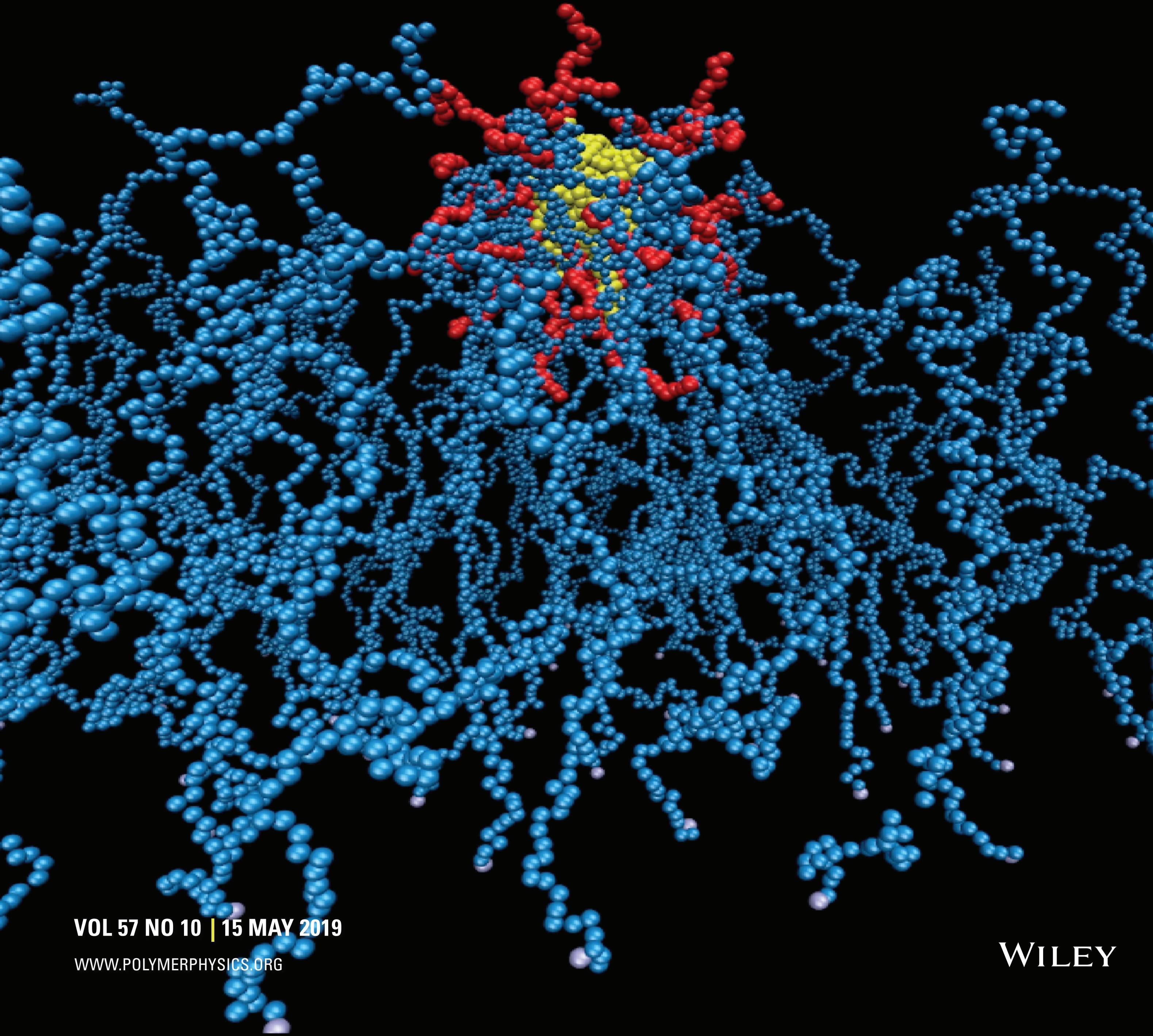

VOL 57 NO 10 | 15 MAY 2019

WWW.POLYMERPHYSICS.ORG

WILEY

Directed Motion of a Polyelectrolyte Micelle along Tethered Chains of Oppositely Charged Polyelectrolyte Brush

Kalliopi Miliou,[1] Leonidas N. Gergidis,[2] Costas Vlahos [1]
[1]Department of Chemistry, University of Ioannina, 45110 Ioannina, Greece
[2]Department of Materials Science & Engineering, University of Ioannina, 45110 Ioannina, Greece
Correspondence to: C. Vlahos (E-mail: cvlahos@uoi.gr)

Received 16 January 2019; accepted 11 March 2019; published online 29 March 2019
DOI: 10.1002/polb.24818

ABSTRACT: The complexation of different single polyelectrolyte (PE) micelles formed by linear diblock copolymers with oppositely charged brushes with varying grafting densities and charge content was studied by means of molecular dynamics simulations using the primitive model. We found that all micelles perform a directed motion along the vertical *z* axis on the grafted surface where they trapped while on the other axes the motion is restricted in a circle in which the diameter decreases with the increase of the hydrophilic length of the linear diblock copolymer. The motion of micelles is characterized as super diffusion inside brushes with low densities and low charge content. At high grafting densities and charge content the diffusion becomes Fickian or slightly subdiffusive. The number of the absorbed brush chains on the micelle corona increases almost monotonically with the increase of brush grafting density or with the decrease of charge content. The distance from the surface in which the micelle is trapped can be controlled by the charge density along the grafted PE chain. © 2019 Wiley Periodicals, Inc. J. Polym. Sci., Part B: Polym. Phys. **2019**, *57*, 621–631

KEYWORDS: brushes; micelles; molecular dynamics; polyelectrolytes

INTRODUCTION The understanding of the complexation of micelles or proteins with oppositely charged polyelectrolyte (PE) brushes is of fundamental importance in various scientific fields especially in the design of efficient artificial enzymes for environmental, industrial, medical, and biosensing applications.[1–3] The reason is that the immobilization through complexation of micelles (artificial enzymes) or proteins (natural enzymes) into spherical or planar brushes enhances the stability in various environments[3] and induces enzyme selectivity because substrates with different sizes have different diffusion characteristics into immobilization media and consequently different performances in catalytic reactions.[4]

Experimental studies on the immobilization of bovine serum albumin protein in a spherical poly(acrylic acid) brush reveal an interesting directed sliding motion of protein along the tethered chains.[5] This result has been concluded from the fact that the total amount of adsorbed protein determined from the analysis of the small-angle X-ray scattering data increases with the time as $t^{0.25}$ and not as $t^{0.5}$ as expected for a purely diffusive transport. The electrostatic interaction increases when the proteins are moving from outside into the brush layer along the radial direction and the proteins are driven into the brush by the inhomogeneous electric field.

Despite the extensive study[3,5–9] of the immobilization through complexation of proteins in spherical and planar PE brushes little is known about the complexation and the kinetics of micelles into opposite charged PE brushes. In previous paper,[10] using molecular dynamics simulations, we predicted the structural and electrical characteristics of PE micelles formed by diblock copolymers with one charged block A and one solvophobic block B. In particular, A_5B_{30}, $A_{10}B_{30}$, and $A_{20}B_{30}$ having 5, 10, 20 charged, and 30 solvophobic units were studied using the Primitive model (spherical charged particles and implicit solvent). The mean aggregation number, the shape, the electrical potential as a function of the distance of the micelle's center of mass (CM), and the zeta potential were calculated at different Bjerrum lengths. The results were in full agreement with experimental and other theoretical findings.[11,12] In another research work, we studied the conformational properties of brushes formed by PE polymers tethered on a planar surface.[13] Using molecular dynamics simulations, the diagram of states characterized by a different degree of condensed counterions inside the brush volume, the chain stretching, and grafting density was constructed for salt free solutions. The simulation results for the height *H* of the brush for the osmotic and the charged regimes were found in good agreement with existing analytical results.[14]

Additional Supporting Information may be found in the online version of this article.

The objective of the current work is the study of the complexation and the kinetics of a single PE micelle of the Types A_5B_{30}, $A_{10}B_{30}$, and $A_{20}B_{30}$ with a brush formed by opposite charged tethered linear chains. We employed molecular dynamics simulation using the Primitive model with Langevin thermostat in order to elucidate the effects of the grafted chains charged units ratio α, the brush grafting density and the micelle size and charge on their complexation. The properties of interest are the radius of gyration of the micelle the mean number of complexed brush units and chains on the micelle surface and the mean square displacement (MSD) of single micelle CM. The simulations are conducted at Bjerrum length $l_B = 1\sigma$ corresponding to water solvent for our model.

MODEL

Modeling of the Brush

We employed a coarse-grained model in order to study linear PE polymers. A group of atoms were modeled as a unit with a diameter σ. A fraction α of units of the PE linear chain, assigned randomly, is charged with elementary quenched charge $+1e$. For chain charge neutralization, counterions with a diameter σ carrying elementary opposite charge $-1e$ are also added to the PE linear system.

The substrate surface for our PE linear polymer brushes is taken to be a piece of the *xy* plane with linear dimensions $L \times L$ and periodic boundary conditions applied in *x* and *y* directions. We consider 64 replicated linear chains root tethered on the plane and the respective counterions. The grafting separation distance between PE chains is set equal to δ in both *x* and *y* directions shown in Figure 1. The surface area per linear chain *s* is calculated as $s = \delta^2$ and, therefore, the grafting density is specified by $d = 1/s = 1/\delta^2$.

Electrostatic interaction between two charged particles q_i and q_j is determined by the Coulomb potential[15]

$$U(r_{ij}) = k_B T l_B \frac{q_i q_j}{r_{ij}} \tag{1}$$

where r_{ij} is the center-to-center distance between charged species. The Bjerrum length is defined as $l_B = e^2/(4\pi\varepsilon_0\varepsilon_r k_B T)$, where ε_0 and ε_r are the permittivity of the vacuum and the relative permittivity of the solvent, respectively.

In addition to the electrostatic interaction, bead–bead interactions were considered, in order to mimic the macroscopic solvent conditions. These interactions are calculated by means of a truncated Lennard–Jones potential:[15,16]

$$U_{LJ}(r_{ij}) = \begin{cases} 4\varepsilon\left[\left(\frac{\sigma}{r_{ij}}\right)^{12} - \left(\frac{\sigma}{r_{ij}}\right)^{6} - \left(\frac{\sigma}{r_{\mathrm{cij}}}\right)^{12} + \left(\frac{\sigma}{r_{\mathrm{cij}}}\right)^{6}\right], r_{ij} \le r_{\mathrm{cij}} \\ 0, r_{ij} > r_{\mathrm{cij}} \end{cases} \tag{2}$$

where ε is the well-depth, and r_{cij} is the cutoff radius. The surface is considered as a reflecting wall. Different units of a linear chain were connected with finitely extensible nonlinear elastic (FENE) bonds. The FENE potential is expressed as[15,16]

$$U_{\mathrm{Bond}}(r_{ij}) = \begin{cases} -0.5kR_0^2 \ln\left[1-\left(\frac{r_{ij}}{R_0}\right)^2\right], r_{ij} \le R_0 \\ \infty, \qquad r_{ij} > R_0 \end{cases} \tag{3}$$

where r_{ij} is the distance between units *i* and *j*, $k = 25\varepsilon/\sigma^2$, and R_0 is the maximum extension of the bond ($R_0 = 1.5\sigma$). These parameters[13,16] prevent chain crossing by ensuring an average bond length of 0.97σ.

The solvent molecules are implicitly considered. The model allows the statistical treatment of the solvent, incorporating its influence on the polymer by a combination of random forces and frictional terms. The friction coefficient and the random force couple the simulated system to a heat bath and therefore the simulation has canonical ensemble Please expand NVT and LAMMPS. (NVT) constraints. The equation of motion of each unit *i* of mass *m* in the simulation box follows the Langevin equation[10]

$$m_i \ddot{\boldsymbol{r}}_i(t) = -\boldsymbol{\nabla}\sum_j \left[U_{LJ}(r_{ij}) + U_{\mathrm{Bond}}(r_{ij}) + U_{\mathrm{Coulomb}}(r_{ij})\right] - m_i\xi\dot{\boldsymbol{r}}_i(t) + \boldsymbol{F}_i(t) \tag{4}$$

where m_i, $\boldsymbol{r}_i$, and ξ are the mass, the position vector, and the friction coefficient of the *i* unit, respectively. The friction coefficient is equal to $\xi = 0.5\tau^{-1}$, with $\tau = \sigma\sqrt{m/\varepsilon}$. The random force vector $\boldsymbol{F}_i$ is assumed to be Gaussian, with a zero mean, and satisfies the equation

$$\left\langle \boldsymbol{F}_i(t)\cdot\boldsymbol{F}_j(t')\right\rangle = 6k_B T m\xi\delta_{ij}\delta(t-t'), \tag{5}$$

where k_B is the Boltzmann constant and *T* is the temperature.

Grafted PE linear polymers are simulated with a length of 160 units and a charge fraction α of charged units varying from 0.05 (α0.05) to 0.75 (α0.75). The Bjerrum length l_B, which determines the strength of electrostatic interactions, was set to 1σ which corresponds to water solvent for our model. We have omitted the spaces and the "=" character, in the notation. Thus, $\alpha0.2d0.031$ is the brush containing PE linear chains with a fraction of charged units $\alpha = 0.2$, and grafted density $d = 0.031\sigma^{-2}$.

Molecular dynamics simulations with Langevin thermostat were performed using the open-source massive parallel simulator LAMMPS.[17] Long-range electrostatic interaction was taken with cutoff $r_{\mathrm{cij}} = 5\sigma$ using a particle–particle particle–mesh (PPPM) method[13,18] for the slab geometry implemented in LAMMPS with a charge interpolation scheme. An estimated accuracy of 10^{-4} was used for calculations of the electrostatic interactions between all charges in the system. The method allows a PPPM solver to be used for systems that are periodic in *x*,*y* but nonperiodic in *z*. This is done by treating the system as periodic in *z*, by inserting empty volume between atom slabs and removing dipole interslab interactions, so that slab–slab interactions are effectively turned off. The

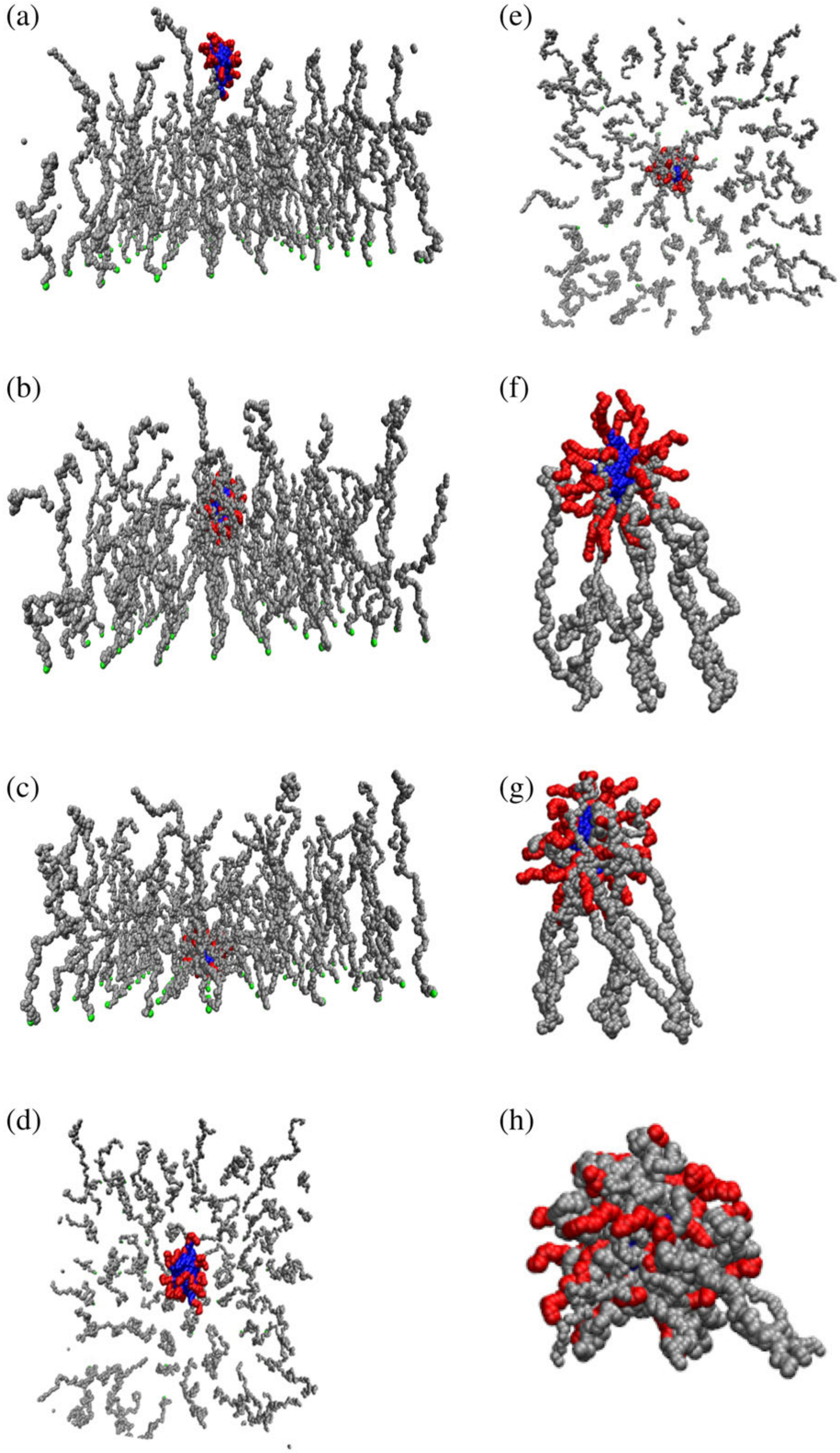

FIGURE 1 Simulation snapshots: (a,d) Initial placement of $A_{10}B_{30}$ micelle on the brush. (b,e) The $A_{10}B_{30}$ micelle inside the brush. (c) The $A_{10}B_{30}$ micelle trapped on the surface. (f–h) The $A_{20}B_{30}$ micelle in the intake, diffusive, and trapped regimes. For clarity, only some of the complexed brush chains are shown. Counterions are omitted in the snapshots. The brush is the $\alpha 0.2 d 0.003$. [Color figure can be viewed at wileyonlinelibrary.com]

distance between two-dimensional periodic images along the z direction was set as $L = 3L_z$.

The reduced temperature T^* of the simulation was set $T^* = k_BT/\varepsilon = 1.1$ and this choice is explained in detail in the next section. The interactions between polymer units, counterions, and the respective interactions of counterions with polymer units were considered always repulsive with cutoff radii $r_{\mathrm{cij}} = 2^{1/6}\sigma$ and are independent from the temperature of the system. For the sake of simplicity, the beads and the counterions were considered to have the same mass ($m = 1$) and diameter ($\sigma = 1$). In all simulations we set $\varepsilon = 1$.

Brushes with 64 PE linear chains with varied grafting density values ranging from $d = 0.002\sigma^{-2}$ up to $d = 0.031\sigma^{-2}$ were simulated. In the initial configuration, each counterion is located in close proximity with a charged monomer. The L_z simulation box dimension along z axis was 200σ for brushes with $d = 0.002\sigma^{-2}$ and longer for the other cases, in order to ensure that the total volume fraction of polymer units and counterions will be constant. The integration time step was $\Delta t = 0.006\tau$. We performed 1 million time steps with all cutoff radii set equal to $r_{\mathrm{cij}} = 2^{1/6}\sigma$, in order to eliminate any bias introduced from the initial conformation. The system then was allowed to equilibrate for another million steps. The production phase of the simulation subsequently conducted for 3 million steps. The properties of interest were calculated from 1000 snapshots of the simulated system.

Modeling of a Single Micelle

The three different single micelles used in this work for the study of complexation with the positive charged brushes were obtained from our previous simulations[10] from a sample of 1000 copolymer chains at the reduced temperature $T^* = 1.8$ and total copolymer and counterions volume fraction $\Phi = 12\%$. Namely, micelles formed by A_5B_{30}, $A_{10}B_{30}$, and $A_{20}B_{30}$ linear diblock copolymers having one fully negative charged A block with 5, 10, 20 units, and one solvophobic with 30 units, respectively, were considered. The aggregation numbers of micelles were $N_p = 29$, 23, and 25, respectively, identical to the preferential aggregation numbers of these systems.

The stability of the micelle strongly depends on the reduced temperature and the volume fraction of the system.[16] Since the volume fraction of the tethered PE polymers and counterions of the brush is around $\Phi = 0.4\%$, it is necessary to reduce the temperature of the system in order to retain the size and the aggregation number of the micelle close to this particular volume fraction value. Different cutoff distances in the Lennard–Jones potential were used[16,19] to describe the interactions between copolymer units. The B–B interaction had an attractive potential with cutoff radius $r_{\mathrm{cij}} = 2.5\sigma$, while the A–A, A–B, A-counterion, B-counterion, and counterion–counterion interactions were considered repulsive having cutoff radii $r_{\mathrm{cij}} = 2^{1/6}\sigma$. The long-range electrostatic interactions between the negatively charged A beads and the respective between A beads and counterions were handled using the PPPM method.[10] The Bjerrum length value was set $l_B = 1\sigma$ corresponding to water solvent.[10] Using these interaction parameter values between all type units and counterions, the simulation was repeated with time step $\Delta t = 0.006\tau$ in a cubic box having exactly the same volume with the free volume of the box that we have used in the simulation of PE brush. It is verified that the reduced temperature $T^* = 1.1$ is the appropriate temperature of the system. Accordingly, all micelles retain their aggregation number up to 2.200.000 time steps. Later on, the $A_{20}B_{30}$ micelle with the higher solvophilic content loses one copolymer chain and remains in equilibrium with the single copolymer chain. With the same criterion[20] the temperature $T^* = 1.8$ was chosen as the appropriate temperature for the study of micelles in solutions with $\Phi = 12\%$.

RESULTS AND DISCUSSION

The Isolated PE Brush

Before focusing on the complexation of micelles A_5B_{30}, $A_{10}B_{30}$, and $A_{20}B_{30}$ with the opposite charged PE brushes, it would be necessary to illustrate the conformation of isolated PE brushes used in this work first. The results are presented in Table 1. The distance $\delta = 1/(d^{1/2})\sigma$ between successive tethered chains of the brush was varied from 0.3 to 1.2 times the diameter of the $A_{10}B_{30}$ micelle which has an intermediate size compared to the A_5B_{30} and $A_{20}B_{30}$ micelles. For spherical objects like present micelles with shape anisotropy parameter κ^2 values varying between 0.02

TABLE 1 The Radii of Gyration$\langle Rg_{xy}^2\rangle$, $\langle Rg_z^2\rangle$, the Span <R>, the Height *H*, the Percentage of Confined Counterions, and the Zeta Potential for Brushes at Different Charged Units Ratio α and Grafting Densities *d*. All Grafted Chains Contain 160 Beads

Brush	$\langle Rg_{xy}^2\rangle/\sigma^2$	$\langle Rg_z^2\rangle/\sigma^2$	$\langle R\rangle/\sigma$	H/σ	Confined Counterions (%)	Zeta Potential V
α0.2*d*0.002	40 ± 1	271 ± 7	55 ± 1	60 ± 1	92.7 ± 0.3	–
α0.2*d*0.003	42 ± 1	273 ± 7	55.5 ± 0.8	59.7 ± 0.5	93.9 ± 0.6	–
α0.2*d*0.004	39 ± 2	274 ± 14	55 ± 2	60 ± 1	95.0 ± 0.9	–
α0.2*d*0.005	38 ± 2	281 ± 16	56 ± 1	60 ± 1	95.9 ± 0.9	0.179
α0.2*d*0.008	36 ± 2	280 ± 13	55 ± 1	60 ± 1	97.2 ± 0.7	0.126
α0.2*d*0.014	33 ± 2	292 ± 16	56 ± 2	62 ± 2	98.2 ± 0.5	0.08
α0.2*d*0.031	31 ± 1	330 ± 13	59 ± 1	65 ± 1	99.0 ± 0.2	0.042
α0.75*d*0.002	40 ± 1	691 ± 19	88 ± 3	92 ± 2	97.4 ± 0.1	0.166
α0.5*d*0.002	37 ± 1	541 ± 17	77 ± 2	81 ± 2	96.7 ± 0.1	0.204
α0.05*d*0.002	56 ± 2	92 ± 3	34.3 ± 0.8	35 ± 1	79 ± 2	–
α0.2(80_20)*d*0.005	42 ± 2	248 ± 11	51 ± 2	61 ± 2	96.1 ± 0.6	0.174
α0.2(20_80)*d*0.005	52 ± 4	260 ± 18	53 ± 2	52 ± 2	96.4 ± 0.7	0.145

and 0.06, the actual micelle diameter is equal to $2\sqrt{5\left\langle R_g^2\right\rangle/3}$, where $\left\langle R_g^2\right\rangle$ is the mean square radius of gyration of the whole micelle.

For brushes with charged units ratio $\alpha = 0.2$ it is observed that the increase of the grafting density from $d = 0.002\sigma^{-2}$ to $0.014\sigma^{-2}$ has no effect on the brush height H which remains constant having a value around 60σ. Only at the highest density $d = 0.031\sigma^{-2}$ H increases up to 65σ. The independence of brush height from the brush grafting density is a basic characteristic of the osmotic regime.[14] Indeed, the percentage of the total number of counterions that are confined inside the brush volume from the surface and up to the external Helmholtz plane[10,21] (Stern layer) vary from 93 to 99% revealing that the aforementioned brushes are in the osmotic regime.[13] The values of the span of the tethered chains <*R*> and those of the brush height *H* differ less than 10% indicating that the tethered chains are almost perpendicular to the grafting surface. This can be revealed from the comparison of the tethered PE chain radius of gyration components. $\left\langle Rg_z^2\right\rangle$ and $\left\langle Rg_{xy}^2\right\rangle$ describing the size of the chain projections to the *xy* plane and the *z* axis, respectively. The $\left\langle Rg_z^2\right\rangle$ values are one order higher than the respective $\left\langle Rg_{xy}^2\right\rangle$ values.

The zeta potential of the PE brushes was calculated by solving numerically the Poisson equation[22] with the appropriate boundary conditions and asymptotics.[23] The method was described in detail in a previous paper[10] and is efficient for brushes with high charge densities. Thus, the electric characteristics of low grafting density brushes having small charged units ratio values α are not reported in Table 1. It is observed that the percentage of confined counterions inside the Stern layer decreases as the grafting density decreases. This leads to the increase of the net charge of the brush and consequently to the increase of zeta potential.

The next category of brushes studied are those with a constant grafting density $d = 0.002\sigma^{-2}$ and varying fraction of charged units $\alpha = 0.05$, 0.2, 0.5, and 0.75. From Table 1 is observed that the brushes with $\alpha = 0.2$, 0.5, and 0.75 are in the osmotic regime since the percentages of confined counterions in the Stern layer varies from 93 to 98%. In the last brush with $\alpha = 0.05$, the percentage of confined counterions is 79% and the brush belongs to the charged regime. The variation of the percentage of confined counterions reflects to the zeta potential values which decrease with the increase of charged units ratio α. The height of brushes *H* increases significantly with the increase of α taking the values of 35σ and 92σ for $\alpha = 0.05$ and 0.75, respectively.

In all the aforementioned brushes, the charged units were randomly distributed along the tethered chain. In order to study the effects of significant charge asymmetry distribution of the grafted chains on the complexation with opposite charged micelles two extra brushes the α0.2(80_20)d0.005 and α0.2(20_80)d0.005 were considered. In the first one, the 80% of the total charged units were randomly distributed along the first half length of the tethered chain (starting from the tethered unit) while the rest 20% of the total charge is randomly distributed on the second half of the tethered chain. In the second brush, the distribution of charges is the reverse. The results are listed in Table 1. We found that the height, the number of confined counterions, and the zeta potential of the α0.2(80_20)d0.005 brush are almost the same with the respective values of the α0.2d0.005 brush. In contrast, the height and the zeta potential of α0.2(20_80)d0.005 brush are smaller despite the fact that the values of the span of the tethered chains and percentage of the confined counterions in the Stern layer are the same with the other two brushes α0.2 (80_20)d0.005 and α0.2d0.005.

The Isolated PE Micelle

The conformational characteristics of the single A_5B_{30}, $A_{10}B_{30}$, and $A_{20}B_{30}$ micelles used in this study are listed in Table 2 for the two different reduced temperatures $T^* = 1.8$ and 1.1. The shape anisotropy κ^2 is defined[10] as $\kappa^2 = 1 - 3\langle I_2\rangle/\langle I_1^2\rangle$, where I_1 and I_2 are the first and the second invariants of the radius of gyration tensor. The value of $\kappa^2 = 0$ corresponds to perfect sphere while $\kappa^2 = 1$ to perfect rod.

It can be observed that at $T^* = 1.1$, the percentage of the confined counterions inside the Stern layer of the micelle is enormously reduced compared to $T^* = 1.8$ and all micelles are in the charged regime. This results in the increase of micelle corona size since the repulsive Coulomb interactions increase the expansion the solvophilic A blocks. The size of the micelle core depends on the length and the charge of the A blocks. In the A_5B_{30} and $A_{10}B_{30}$ micelles, the $<Rg^2>_{\text{core}}$ values become

TABLE 2 The Aggregation Number N_p, the Radii of Gyration $<\text{Rg}^2>_{\text{micelle}}$, $<\text{Rg}^2>_{\text{core}}$, the Shape Anisotropy Parameter κ^2, and the Percentage of Confined Counterions Inside the Stern Layer of the Micelles at Different Reduced Temperatures T^*. All Solvophilic Units Are Charged ($\alpha = 1$)

Micelle	N_p	$<Rg^2>_{\text{micelle}}/\sigma^2$	$<Rg^2>_{\text{core}}/\sigma^2$	$\kappa^2_{\text{micelle}}$	κ^2_{core}	Confined Counterions (%)	Temperature T^*
A_5B_{30}	29	43.8	36.2	0.07	0.09	70	1.8
$A_{10}B_{30}$	23	52.5	28.4	0.06	0.09	70	1.8
$A_{20}B_{30}$	25	80.9	29.2	0.01	0.05	92	1.8
A_5B_{30}	29	35.2 ± 0.2	26.7 ± 0.2	0.024 ± 0.003	0.031 ± 0.005	42	1.1
$A_{10}B_{30}$	23	51 ± 1	25.3 ± 0.8	0.03 ± 0.01	0.06 ± 0.02	50	1.1
$A_{20}B_{30}$	25	123 ± 4	31 ± 2	0.02 ± 0.01	0.09 ± 0.05	49	1.1

smaller than the respective values at $T^* = 1.8$ while in $A_{20}B_{30}$, the protection of the solvophobic units is more robust than at $T^* = 1.1$ and the $<Rg^2>_{core}$ values increase. Overall, the $A_{10}B_{30}$ micelle retains its size in both temperatures while the size of the A_5B_{30} and $A_{20}B_{30}$ micelles at $T^* = 1.1$ becomes smaller and higher compared to the respective sizes at $T^* = 1.8$. All micelles at $T^* = 1.1$ are spherical with shape anisotropy parameter κ^2 values around 0.02.

Complexation of Micelle with Opposite Charged Brush

The last configuration of the production run of PE brushes was considered as the initial conformation in the simulation of micelle complexation. The PE micelle was obtained from our previous simulations[10] at the reduced temperature $T^* = 1.8$ and placed close to the brush height in a way to avoid any overlapping with the brush units and counterions [Fig. 1(a,d)]. The micelle conformation at $T^* = 1.8$ was chosen because the majority of counterions are confined inside the micelle radius and this facilitates the micelle placement above the brush. The simulation of the positively charged brush with negatively charged micelle was performed at $T^* = 1.1$ using the values of interaction parameters, Bjerrum length, time step as described in the model section. The long-range electrostatic interactions were handled using the PPPM method for the slab geometry. Each simulation was conducted at least for 3.000.000 and up to 10.000.000 time steps for brushes with high grafting density d and high charged units ratio α. The properties of interest were calculated as averages from 3000 snapshots. The variation of the radii of gyration of A_5B_{30}, $A_{10}B_{30}$, and $A_{20}B_{30}$ micelles with the time during the complexation with the $\alpha0.2d0.014$ brush is presented in Figure 2. After a small elapsed time, even before the complexation with the brush in many cases, the radius of gyration of the micelle attains the respective equilibrium values of the isolated micelle for the temperature $T^* = 1.1$. When the micelle gradually enters inside the brush, the number of the complexed units of the micelle increases reaching a limiting value when the micelle lies deep inside the brush. The correlations between complexed units induce attractions[24] resulting in the worsening of the solvent quality. Consequently, the shrinking of micelle radius of gyration up to its equilibrium value is reached. Similar variation of the radii of gyration of micelles is observed in the complexation with brushes of different grafting densities. The equilibrium values of the micelles radii of gyration are listed in Table 3. It is observed that in complexation with brushes having charged units ratio $\alpha = 0.2$, the values of the radii of gyration $<Rg^2>_{micelle}$ and $<Rg^2>_{core}$ remain constant independent of the brush grafting density. The aforementioned values compared to the respective values of the isolated micelles at the same temperature $T^* = 1.1$ are smaller about 6, 15, and 25% for the A_5B_{30}, $A_{10}B_{30}$, and $A_{20}B_{30}$ micelles, respectively. The number of the absorbed brush chains on the micelle corona (Table 3) increases almost monotonically with the increase of brush grafting density because the number of brush chains in the vicinity of micelle increases. However, the total number of complexed units of micelle with the opposite charged brush units remain constant with the increase of grafting density. We verified that the ratio between the number of complexed units of two different micelle types A_5B_{30}, $A_{10}B_{30}$, or $A_{20}B_{30}$ at any brush density is equal to the ratio of the total charges of the isolated micelles. As the total charge, we consider the charge of the fully ionized micelle (145 charges for the A_5B_{30}).

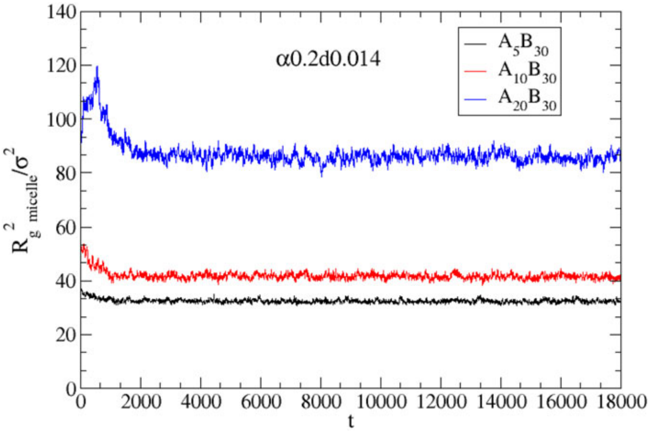

FIGURE 2 The variation of radii of gyration of A_5B_{30}, $A_{10}B_{30}$, and $A_{20}B_{30}$ micelles with the time during the complexation with the $\alpha0.2d0.014$ brush. [Color figure can be viewed at wileyonlinelibrary.com]

The motion of the A_5B_{30}, $A_{10}B_{30}$, and $A_{20}B_{30}$ micelles CM along the three coordinate directions as a function of time is illustrated in Figure 3 for brushes with $\alpha = 0.2$ and different grafting densities. A first striking observation on these plots is that all micelles follow a directed motion along the vertical z axis on the grafted surface while on the other axes the motion is restricted. Similar directed motion was detected experimentally in proteins adsorption into spherical PE brushes.[5] The decay of z component of micelles CM with the time and the associated motion may characterized by three distinct regimes. The intake regime which is relatively fast, the diffusive regime, where the micelle is completely encapsulated and diffuses inside the brush [Fig. 1(b)] and the trapped regime, where the micelle CM moves very slowly approaching the grafting surface and is trapped on it [Fig. 1(c,e,h)]. Additional simulations were performed in order to clarify the mechanism of the micelle complexation with the opposite charged brush using the following system: a single fully extended grafted chain with $\alpha = 0.2$. The A_5B_{30} micelle was attached to the free end unit of the grafted chain.

In the first simulation, the grafted chain was modeled to be completely stiff while in the other was allowed to be flexible. In the case of stiff grafted chain, it is found that the micelle follows one-dimensional random walk motion along the chain contour while in the other case the flexible chain was wrapped around the micelle continuously forcing the micelle in a directed rotational motion toward the surface where it is trapped. The micelle performs a directed motion toward the surface because for the opposite direction motion there is an entropic penalty arising from the necessity of unwrapping the grafted chain from the micelle. In the case of PE brush, many chains simultaneously are enfolded around the micelle (Fig. 1). The directed motion of the A_5B_{30}, $A_{10}B_{30}$, and $A_{20}B_{30}$ micelles CMs is restricted in a tube with small diameter which decreases as the brush grafting density increases (Fig. 4). For

TABLE 3 The Size and the Shape Anisotropy of A_5B_{30}, $A_{10}B_{30}$, and $A_{20}B_{30}$ Micelles Core and the Whole Micelle, the Number of Absorbed Brush Chains on the Micelle, and the Number of the Complexed Micelle Units Inside Brushes of Different Grafting Densities d and Charged Units Ratio α

Micelle	$\langle Rg^2\rangle_{micelle}/\sigma^2$	$\langle Rg^2\rangle_{core}/\sigma^2$	$\kappa^2_{micelle}$	κ^2_{core}	Number of Absorbed Chains	Number of Complexed Units
A_5B_{30}						
α0.2d0.002	32.8 ± 0.6	25.5 ± 0.4	0.017 ± 0.005	0.022 ± 0.005	7.0	25.4
α0.2d0.003	32.8 ± 0.6	25.5 ± 0.4	0.017 ± 0.004	0.022 ± 0.005	8.0	25.5
α0.2d0.004	32.6 ± 0.5	25.3 ± 0.3	0.015 ± 0.003	0.019 ± 0.004	7.6	25.7
α0.2d0.005	32.6 ± 0.3	25.3 ± 0.2	0.016 ± 0.003	0.020 ± 0.004	9.1	25.7
α0.2d0.008	32.6 ± 0.4	25.3 ± 0.2	0.016 ± 0.003	0.020 ± 0.004	10.6	25.9
α0.2d0.014	32.5 ± 0.3	25.4 ± 0.2	0.017 ± 0.004	0.022 ± 0.004	12.1	27.3
α0.2d0.031	32.2 ± 0.2	25.2 ± 0.1	0.016 ± 0.002	0.020 ± 0.002	20.0	39.0
$A_{10}B_{30}$						
α0.2d0.002	43 ± 2	22.4 ± 0.8	0.018 ± 0.009	0.03 ± 0.02	10.5	44.3
α0.2d0.003	42 ± 2	22.3 ± 0.9	0.016 ± 0.009	0.03 ± 0.01	10.2	45.2
α0.2d0.004	42 ± 2	22.3 ± 0.7	0.017 ± 0.009	0.03 ± 0.02	12	44.6
α0.2d0.005	42 ± 2	22.3 ± 0.9	0.02 ± 0.02	0.03 ± 0.03	12.2	45.1
α0.2d0.008	42 ± 1	22.2 ± 0.4	0.016 ± 0.004	0.027 ± 0.006	13.1	46.2
α0.2d0.014	42.0 ± 0.9	22.2 ± 0.4	0.017 ± 0.005	0.03 ± 0.01	16.8	47.1
α0.2d0.031	41.1 ± 0.9	21.9 ± 0.4	0.015 ± 0.006	0.025 ± 0.009	26.6	63.9
$A_{20}B_{30}$						
α0.2d0.002	95 ± 6	24.9 ± 0.9	0.042 ± 0.02	0.06 ± 0.01	18.6	98.5
α0.2d0.003	93 ± 7	25 ± 1	0.04 ± 0.01	0.05 ± 0.03	19.9	100.2
α0.2d0.004	91 ± 6	24 ± 1	0.023 ± 0.008	0.04 ± 0.02	21.1	102.1
α0.2d0.005	89 ± 4	23.8 ± 0.6	0.02 ± 0.01	0.04 ± 0.01	22.1	104.1
α0.2d0.008	89 ± 6	23.8 ± 0.9	0.015 ± 0.006	0.03 ± 0.01	23.8	104.4
α0.2d0.014	87 ± 4	23.6 ± 0.7	0.014 ± 0.007	0.03 ± 0.02	29.5	107.4
α0.2d0.031	86 ± 4	24 ± 1	0.014 ± 0.01	0.03 ± 0.03	45.2	145.6
$A_{10}B_{30}$						
α0.75 d0.002	36.5 ± 0.7	21.6 ± 0.3	0.021 ± 0.009	0.02 ± 0.01	4.7	132.6
α0.5 d0.002	38 ± 2	21.8 ± 0.7	0.02 ± 0.02	0.03 ± 0.02	6.1	95.2
α0.05 d0.002	65 ± 11	34 ± 9	0.1 ± 0.1	0.2 ± 0.2	11.8	–
$A_{10}B_{30}$						
α0.2(80_20) d0.005	40 ± 3	22 ± 1	0.02 ± 0.01	0.03 ± 0.02	12.3	64.6
α0.2(20_80) d0.005	38.5 ± 0.4	21.6 ± 0.1	0.014 ± 0.002	0.020 ± 0.003	12.0	66.3

the brush with the highest grafting density $d = 0.031\sigma^{-2}$, the diameter is equal to 10σ, 6σ, and 4σ for the A_5B_{30}, $A_{10}B_{30}$, and $A_{20}B_{30}$ micelles, respectively.

The time needed for a micelle to reach the trapping domain depends on the brush and micelle characteristic. For the same brush, we found that the $A_{20}B_{30}$ micelle reaches faster the trapping domain at grafting surface and the $A_{10}B_{30}$ and A_5B_{30} micelles follow. The increase of grafting density slows down the micelle CM motion leading in higher times. This behavior can be explained as follows: as the micelle charge and size increases, it is easier for the brush chains to enfold the micelle and the directed motion along z axis becomes faster. The increase of the grafting density leads to the increase of the number of brush chains embracing the micelle. However, the number of complexed units per grafted chain decreases

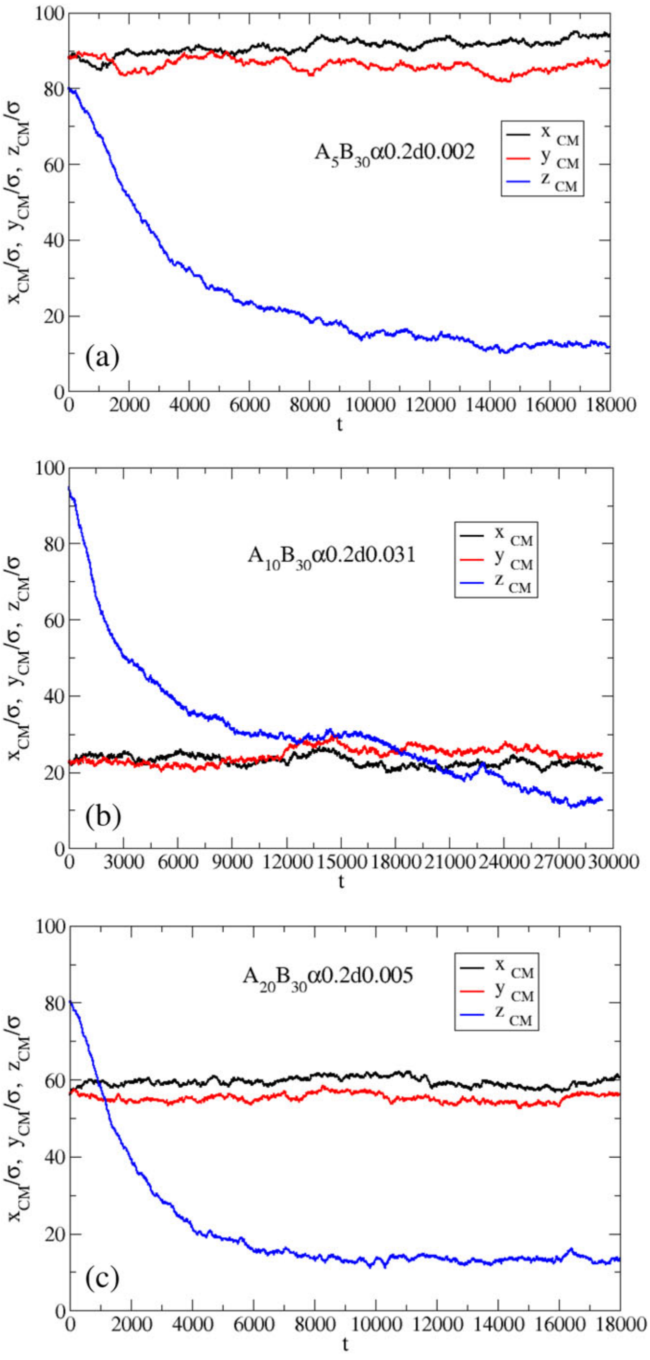

FIGURE 3 CM motion of the (a) A_5B_{30}, (b) $A_{10}B_{30}$, and (c) $A_{20}B_{30}$ micelles along the three coordinate directions as a function of time. [Color figure can be viewed at wileyonlinelibrary.com]

(Table 3) making the embracing of micelles more difficult which leads in the slower motion of the micelles CM. Typical times for A_5B_{30}, $A_{10}B_{30}$, and $A_{20}B_{30}$ micelles for reaching the surface are 14,500, 11,200, 6000, and 44,000, 28,000, 20,000 (in tau units) for the brushes $\alpha0.2d0.002$ and $\alpha0.2d0.031$, respectively.

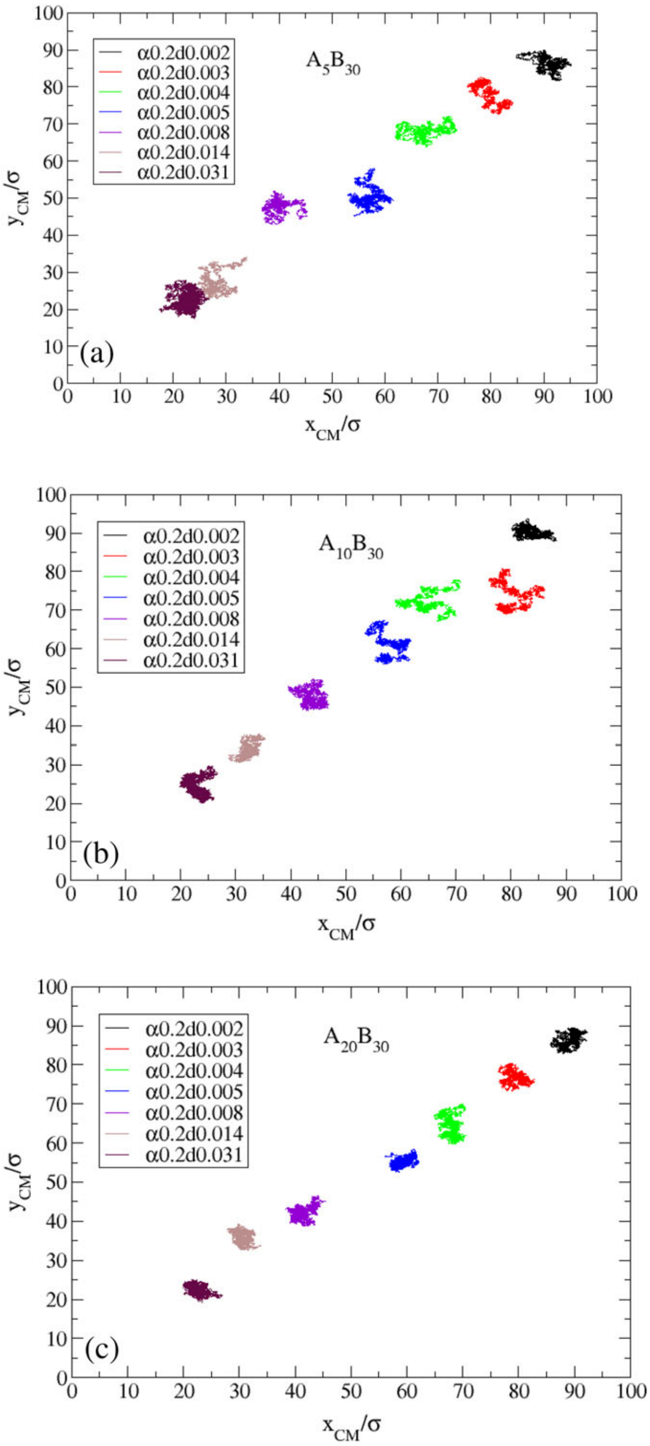

FIGURE 4 The projection of motion of the micelles CM on the *xy* plane parallel to the grafting surface as a function of time for different brushes with $\alpha0.2$. (a) A_5B_{30}, (b) $A_{10}B_{30}$, and (c) $A_{20}B_{30}$ micelles. [Color figure can be viewed at wileyonlinelibrary.com]

For each of the molecular dynamics runs conducted, the micelle CM MSD $< (r_k(t)-r_k(0))^2 >$ was tracked along each coordinate direction k ($k = x,y,z$) as a function of time t. The angular brackets denote averaging over different time origins along the recorded trajectory. Plots of MSD of A_5B_{30}, $A_{10}B_{30}$, and $A_{20}B_{30}$ micelles for the diffusive regime are shown in Figure 5 in logarithmic coordinates. It can be observed that in general, the motion of all micelles inside the brushes with $\alpha = 0.2$ is characterized as superdiffusion since the exponent ω of $\mathrm{MSD} = 2Dt^{\omega}$ is greater than one. Only in the brush $\alpha0.2d0.031$ with the highest grafting density the motion of all micelles becomes Fickian diffusion with $\omega = 1$. For the same brush, we found that the exponent ω takes higher values in the case of A_5B_{30} micelle, lower in $A_{10}B_{30}$, and the lowest values in the case $A_{20}B_{30}$ micelles. The variation of exponent ω with the brush grafting density d is not monotonic as shown in Figure 5(d). In the case of A_5B_{30} micelles, ω increases as the brush grafting density increases up to $d = 0.004\sigma^{-2}$ and then decreases while the inverse behavior is observed in $A_{10}B_{30}$ micelles.

Thereinafter, results on the complexation of the $A_{10}B_{30}$ micelle are presented with $\alpha0.2(80\_20)d0.005$ and $\alpha0.2(20\_80)d0.005$ brushes in which the charged units are not randomly distributed along the contour length of the grafted chains as in the previously studied brushes. In the $\alpha0.2(80\_20)d0.005$ brush, the vast majority of the charged units (80% of them) are placed randomly along the half chain length started from the grafted point while in the rest charged units (20% of the total charge) brush are placed along the second half length of the grafted chain. The $\alpha0.2(20\_80)$ $d0.005$ brush has the inverse distribution of charged units. We found that the charge asymmetry distribution along the PE chain leads in some interesting results regarding the complexation with opposite charged micelle. As observed from Figure 6(a), the $A_{10}B_{30}$ micelle is trapped inside the $\alpha0.2(20\_80)d0.005$ brush (having high charge density close to the brush height) not onto the grafted surface as usual but in certain distance from surface. While the outer part of grafted chains, rich in charges enfolds the micelle moving it deep inside the brush the motion is terminated because the charges on the rest part of the grafted chain (close to the surface) the charges are rare and is difficult for them to enfold the micelle in order to keep the motion toward the surface. The micelle immobilization far away from the surface is important for the efficient operation of artificial enzymes. The $A_{10}B_{30}$ micelle when is complexed with the $\alpha0.2(80\_20)d0.005$ brush is trapped onto the grafted surface where the density of charged units of the grafted chains is higher [Fig. 6(b)**]**. In Table 3, we present the results for the size of $A_{10}B_{30}$ micelle and other properties. It can be observed that the number of grafted chains absorbed on the $A_{10}B_{30}$ micelle is the same for the three brushes $\alpha0.2(20\_80)$ $d0.005$, $\alpha0.2(80\_20)d0.005$, and $\alpha0.2d0.005$. However, the total number of the micelle complexed units in the case of asymmetric charged brushes is about 44% higher compared with the respective number of $\alpha0.2d0.005$ brush. This is reasonable since the micelle is enfolded in the case of asymmetric charged brushes by the part of the grafted chain which is rich in charges when trapped. The higher number of complexed $A_{10}B_{30}$ micelle units results in a small reduction of the micelle radius of gyration compared with the respective value in $\alpha0.2d0.005$ brush due to the correlation-induced attractions, which reduce the solvent quality.

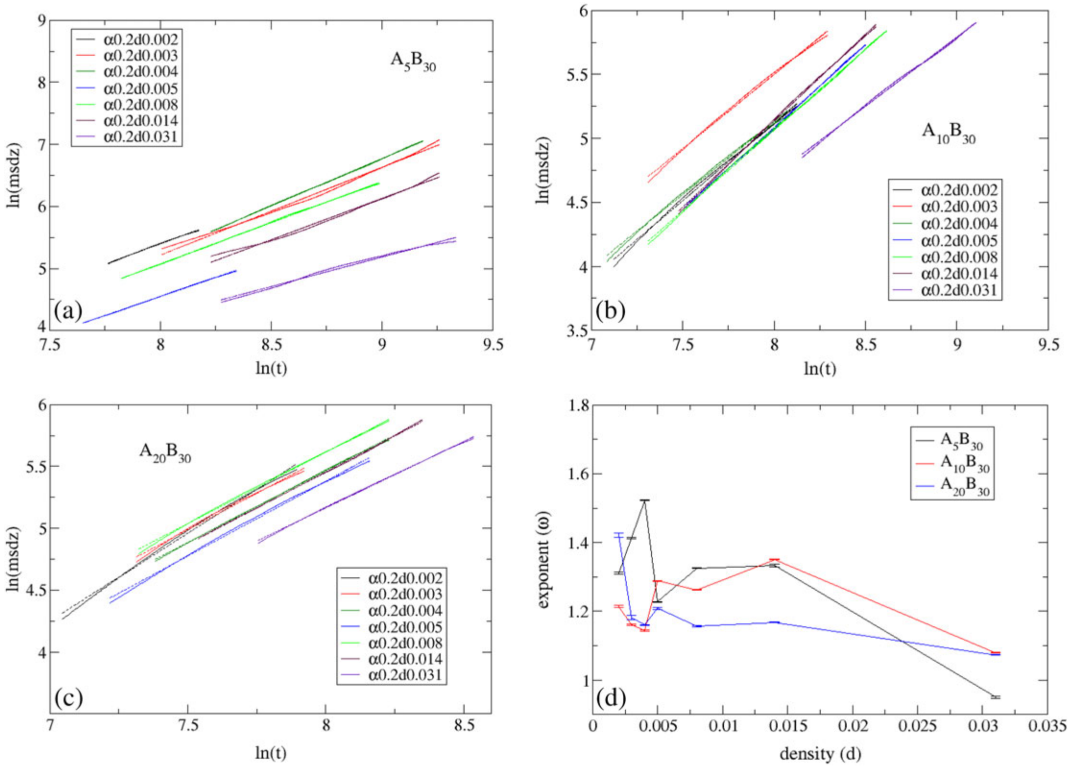

FIGURE 5 Logarithm of MSD in the *z* axis of (a) A_5B_{30}, (b) $A_{10}B_{30}$, and (c) $A_{20}B_{30}$ micelles inside various brushes along the *z* axis as a function of the logarithm of time. The dotted fitting lines are drawn. (d) The resulting slopes and variations. [Color figure can be viewed at wileyonlinelibrary.com]

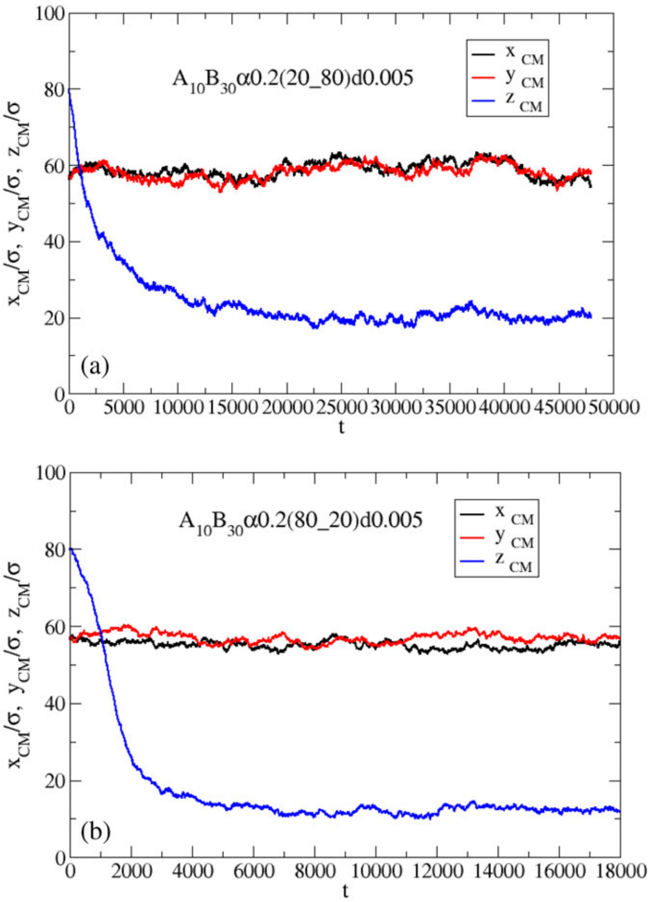

FIGURE 6 CM motion of the $A_{10}B_{30}$ micelle along the three coordinate directions as a function of time for (a) α0.2(20_80) d0.005 and (b) α0.2(80_20)d0.005 brushes. [Color figure can be viewed at wileyonlinelibrary.com]

The last case we studied is the complexation of $A_{10}B_{30}$ micelle with brushes having a constant grafting density $d = 0.002\sigma^{-2}$ and varying charged units ratios $\alpha = 0.75$, 0.5, 0.2, and 0.05. Results regarding the micelle conformation are presented in Table 3**.** It can be observed that the increase of the charged units ratio α lead in the decrease of the number of the brush chains absorbed on the micelle. However, the total number of the complexed units and consequently the number of complexed units per chain significantly increases with the increase of α. This reflects to the decrease of the micelle radii of gyration as α increases from $\alpha = 0.2$ to 0.75 due to the correlation between complexed units which induces attraction worsening the solvent quality. In the case of the α0.05d0.002 brush with $\alpha = 0.05$, however, the micelle radii of gyration and the shape anisotropy parameter κ^2 values are much greater compared to the respective values of the isolated micelle at the same temperature. The height of the α0.05d0.002 brush is small and is just twice the length of the isolated micelle diameter (Tables 1 and 2) and thus the 12 grafted chains complexed with the micelle have their grafting points far apart from the micelle CM. The attractions between the different chains and the micelle lead to the swelling of the micelle and then to the fission of the micelle. Two smaller micelles are formed with aggregation numbers $N_p = 10$ and 13, respectively. The motion of the micelle CM inside the different brushes is illustrated in Figure S1, Supporting Information. It can be seen that the time needed for the micelle to reach the trapped domain on the grafted surface increases with the increase of brush charged units ratio α. From the plot of MSD with the time t (Fig. S2, Supporting Information), it is clear than the motion of the $A_{10}B_{30}$ micelle becomes subdiffusive as the brush charged units ratio α increases. The reason is twofold. When α increases the brush chain becomes stiffer and is difficult to enfold the micelle. On the other hand, as a increases, there are many charged units in a small part of the chain contour that are complexed with the micelle so it becomes difficult for the other charged units in the rest of the grafted chain to find and approach uncomplexed units on the micelle.

CONCLUSIONS

The complexation of a single PE micelle with oppositely charged brushes was studied by means of molecular dynamics simulations with Langevin thermostat using the primitive model at Bjerrum length $l_B = 1\sigma$ corresponding to water solvent for our model. In particular, micelles formed by fully charged A_5B_{30}, $A_{10}B_{30}$, and $A_{20}B_{30}$ linear diblock copolymers with aggregation numbers $N_p = 29$, 23, and 25, respectively, were complexed with brushes consisting of 160 units with ratio of charged units $\alpha = 0.2$ and varying and grafting densities $d = 0.002$, 0.003, 0.004, 0.005, 0.008, 0.014, and $0.031\sigma^{-2}$. We found that all micelles perform a directed motion along the vertical z axis on the grafted surface where they are trapped while on the other axes the motion is restricted in a circle in which the diameter decreases with the increase of the hydrophilic length of the linear diblock copolymer. The motion of all micelles inside the brushes in the diffusive regime is characterized as super diffusion. Only in the brush with the highest grafting density, the motion of all micelles becomes directed Fickian diffusion. For the same brush, we found that the time exponent values of the MSD decreases as the length of the solvophilic block of the diblock copolymer increases. The number of the absorbed brush chains on the micelle corona increases almost monotonically with the increase of brush grafting density. However, the total number of complexed units of micelle with the opposite charged brush units remain constant with the increase of grafting density. We verified that the ratio between the number of complexed units of two different micelle types A_5B_{30}, $A_{10}B_{30}$, or $A_{20}B_{30}$ at any brush density is equal to the ratio of the total charges of the isolated micelles.

In addition, the complexation of $A_{10}B_{30}$ micelle with brushes having different ratios of charged units $\alpha = 0.05$, 0.5, and 0.75 was considered. It is found that the motion of the micelle becomes slightly subdiffusive as the brush ratio of charged units α increases. For the low charged brush with $\alpha = 0.05$, the micelle breaks up during the complexation and two smaller micelles are formed. The distance from the surface in which the micelle is trapped can be controlled from the asymmetry of charge density along the grafted PE chain.

ACKNOWLEDGMENTS

This work was supported by computational time granted from the Greek Research & Technology Network (GRNET) in the National HPC facility—ARIS—under project ID pr004032—polymer brushes.

REFERENCES AND NOTES

1 Y. Lin, J. Ren, X. Qu, *Acc. Chem. Res.* **2014**, *47*, 1097.

2 R. Qu, L. Shen, Z. Chai, C. Jing, Y. Zhang, Y. An, L. Shi, *ACS Appl. Mater. Interfaces* **2014**, *6*, 19207.

3 N. R. Mohamad, N. H. C. Marzuki, N. A. Buang, F. Huyop, R. A. Wahab, *Biotechnol. Biotechnol. Equip.* **2015**, *29*, 205.

4 R. Qu, H. Shi, R. Wang, T. Cheng, R. Ma, Y. An, L. Shi, *Biomater. Sci.* **2017**, *5*, 570.

5 K. Henzler, S. Rosenfeldt, A. Wittemann, L. Harnau, S. Finet, T. Narayanan, M. Ballauff, *Phys. Rev. Lett.* **2008**, *100*, 158301

6 S. Wang, K. Chen, L. Li, X. Guo, *Biomacromolecules* **2013**, *14*, 818.

7 W. M. De Vos, P. M. Biesheuvel, A. De Keizer, J. M. Kleijn, M. A. C. Stuart, *Langmuir* **2008**, *24*, 6575.

8 F. A. M. Leermakers, M. Ballauff, O. V. Borisov, *Langmuir* **2007**, *23*, 3937.

9 N. Gal, M. Schroffenegger, E. Reimhult, *J. Phys. Chem. B* **2018**, *122*, 5820.

10 K. Miliou, L. N. Gergidis, C. Vlahos, *J. Polym. Sci. Part B: Polym. Phys.* **2018**, *56*, 924.

11 E. A. Lysenko, A. I. Kulebyakina, P. S. Chelushkin, A. M. Rumyantsev, E. Y. Kramarenko, A. B. Zezin, *Langmuir* **2012**, *28*, 17108.

12 Y. Lauw, F. A. M. Leermakers, M. A. Cohen Stuart, O. V. Borisov, E. B. Zhulina, *Macromolecules* **2006**, *39*, 3628.

13 K. Miliou, L. N. Gergidis, C. Vlahos, *J. Polym. Sci. Part B: Polym. Phys.* **2017**, *55*, 1110.

14 O. V. Borisov, E. B. Zhulina, *Macromolecules* **2015**, *48*, 1499.

15 A. Kalogirou, L. N. Gergidis, K. Miliou, C. Vlahos, *J. Phys. Chem. B* **2017**, *121*, 1982.

16 N. W. Suek, M. H. Lamm, *Langmuir* **2008**, *24*, 3030.

17 S. Plimpton, *J. Comput. Phys.* **1995**, *117*, 1.

18 R. Ni, D. Cao, W. Wang, A. Jusufi, *Macromolecules* **2008**, *41*, 5477.

19 O. Moultos, L. N. Gergidis, C. Vlahos, *Macromolecules* **2012**, *45*, 2570.

20 O. Moultos, L. N. Gergidis, A. Kalogirou, C. Vlahos, *J. Polym. Sci. Part B: Polym. Phys.* **2015**, *53*, 442.

21 Z. Li, A. K. Van Dyk, S. J. Fitzwater, K. A. Fichthorn, S. T. Milner, *Langmuir* **2016**, *32*, 428.

22 Y. Moroi, *Micelles: Theoretical and Applied Aspects*; Springer Science: New York, **1992**.

23 J. Irigoyen, V. B. Arekalyan, Z. Navoyan, J. Iturri, S. E. Moya, E. Donath, *Soft Matter* **2013**, *9*, 11609.

24 Q. Liao, A. V. Dobrynin, M. Rubinstein, *Macromolecules* **2006**, *39*, 1920.